Understanding a Killer: A Predictive Model for Tumor Development

Yi Jiang

Abstract. Cancer has become the leading cause of death for Americans. The development of prognostic tools could have immediate impact on the lives of millions of cancer patients. We have developed an integrated model that includes a cellular model for cell dynamics (cell growth, division, death, and cell adhesion), an intracellular protein regulatory network for cell cycle control, and extracellular reaction-diffusion chemical dynamics. This model has produced tumor growth dynamics that agree with tumor spheroid experiments. The model has the potential to be a comprehensive and predictive model for tumor development and chemotherapy based on quantitative experiments.

1. Introduction

Since 2002, cancer has overtaken heart diseases and become the leading cause of death for Americans between the ages of 40 and 74 [**1**]. But the overall effectiveness of cancer therapeutic treatments is only 50%. Understanding the tumor biology and developing a prognostic tool could therefore have immediate impact on the lives of millions of people diagnosed with cancer.

Tumor development is very complex and dynamic. The microenvironment inside a tumor, which determines tumor dynamics, involves spatial and temporal variations in nutrient and waste gradients, cellular physiology and viability, energy and macromolecule metabolism, the expression patterns of genes and proteins, as well as the progression of the malignant process. The interplay amongst all of these elements defines the response of a particular tumor to any form of treatment from surgery to the newest wonder drug. Mathematical models based on the underlying tumor growth mechanisms can help the scientific and medical community understand and predict the development of a tumor in different environments and evaluate the potential effectiveness of different approaches for controlling the disease.

The complexity of a tumor *in vivo* has resulted in the development of simpler *in vitro* experimental models of the tumor microenvironment; the primary example has been the multicellular tumor spheroid system. The spheroid system has the great advantage of precisely controlling the external environment while maintaining the cells in a microenvironment that mimics the environment within a solid

2000 *Mathematics Subject Classification.* 92B,92C.

This work has been supported by DOE under Contract W-7405-ENG-36.

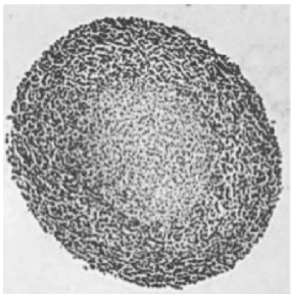

FIGURE 1. A histological cross section through the center of a spheroid 1200 μm in diameter stained with eosin and hematoxalin, showing the viable rim of cells (darker gray) and the necrotic center (light gray).

tumor [**2**]. Suspended in culture, tumor cells aggregate and grow into a spheroid. After initial exponential growth, further spheroid growth progressively slows and eventually stops, even in the presence of a constant nutrient supply [**3**]. A typical spheroid consists of a necrotic (dead) core surrounded by layers of quiescent (alive but not growing, or cell-cycle arrested) and proliferating tumor cells1 [**2**], as shown in Figure 1, in which one can easily distinguish the viable rim of cells surrounding the cellular necrotic core. It is critical to emphasize that this multicellular tumor spheroid experimental model recapitulates all major characteristics of the growth, composition, microenvironment, and therapeutic response of solid tumors in humans [**2**].

This stage of tumor growth, or avascular tumor growth (before vessels), can only reach a few millimeters in diameter. Angiogenesis, formation of new blood vessels from existing blood vessels, is necessary for subsequent tumor expansion. The healthy body controls angiogenesis through angiogenic proteins: angiogenesis growth factors and angiogenesis inhibitors. In a tumor, excessive angiogenesis occurs because of angiogenic growth factors generated by the tumor cells in response to their stressful microenvironment. When these factors diffuse into the nearby tissue, they bind to specific receptors on the endothelial cells of nearby pre-existing blood vessels. The endothelial cells become activated; they proliferate and migrate toward the tumor. Sprouting endothelial cells roll up to form a blood vessel tube. Individual blood vessel tubes connect to form blood vessel loops that can circulate blood. With the new supply system, the tumor will renew growth at a much faster rate. In the metastasis phase, tumor cells use their new blood supply as highways to travel to other parts of the body. In the invasion phase, cells detach from the tumor mass and become motile. They invade the surrounding tissue such that no solid boundary exists between tumor cells and normal tissue.

The desire to understand tumor biology has given rise to mathematical models to describe the tumor development. But no mathematical models of tumor growth yet can start from a single cell and undergo the whole process of tumor development. Most existing models fall in three disconnected regions: avascular tumor growth, angiogenesis, and chemotherapy for tumors with well-established vasculature.

A predictive model of avascular tumor growth has to account for the complexity of these processes. Important elements that need to be incorporated in such

a model include cell proliferation and growth, nutrient consumption and diffusion, waste product production and diffusion, effects of growth promoting and inhibitory factors, intercellular adhesion, and cell-environment interactions, as well as the geometry of the tumor and the cells. Most simple models of tumor growth kinetics have relied on phenomenological curve fitting, such as the Gompertz model [**4**]; more sophisticated ones coupled reaction-diffusion equations governing the chemicals with the tumor growth rate [**5, 6, 7**]. Cellular automata (CA), using a set of oversimplified rules on a lattice, show a qualitative correspondence to real avascular tumor growth [**8**].

For angiogenesis, a number of models, mainly due to Chaplain et al. [**9**], used continuous equations to describe the number of vascular endothelial cells, their interaction with the extracellular matrix, and angiogenic factors. These models reproduced rather realistic average vasculature properties. For the effects of therapy, models often assumed oversimplified tumor and vasculature properties and can only treat a specific effect [**10, 11, 12, 13**].

The only exception is a recent model that simulate the transition from avasular tumor growth to angiogenesis to vascular and invasive growth that employed an adaptive finite-element method coupled to a level-set method [**14**]. However, some effects including cell size changes, the mechanical deformation or compression of cells or cell aggregates, the tumor morphology, and the effects of biochemicals, are hard to capture with a continuous or a simple CA model. A recent model that employs a hybrid of cellular automata for cell representation and continuous equations for chemical and blood flow in a hexagonal grid of blood vessels represents the state of the art in tumor growth modeling [**15, 16**].

In response to the lack of more biologically based models, we have developed a hybrid, multiscale, cellular model of tumor growth [**17**]. The Model section describes our model in three levels: cellular, extracellular, and intracellular. Data from experiments with multicellular spheroids were used to determine the parameters for the simulations. The Results section shows that, starting with a single tumor cell, this model naturally evolves with time to produce an avascular tumor that quantitatively mimics experimental measurements in multicellular spheroids. In the Discussion section, we show the implications of our results. In the Outlook section, we speculate how this multiscale model can be used to model initiation of angiogenesis, vascular tumor growth, and effects of chemotheraphies on different stages of tumor development.

2. Model

Our model consists of three levels: at the cellular level, a Monte Carlo model for cell growth, death, cell cycle arrest, and cell-cell adhesion; at the extracellular: a set of reaction-diffusion equations for chemical dynamics; and at the intracellular: a rudimentary protein regulatory network for controlling cell cycle.

The details of the model is described in [**17**]. Briefly, the cellular model is based on the successful cellular Potts model [**18, 19**]. In this model, lattice space is partitioned into domains of individual cells and cell medium; pixels within each cell have a number S, the ID number of the cell. Figure 2 shows a schematic of the cells. Cell properties include a cell type (e.g., tumor, normal, endothelial), adhesiveness to its neighbors, volume (typically between 125 to 250 pixels), and growth, and metabolic rates. The total energy of the system includes the surface

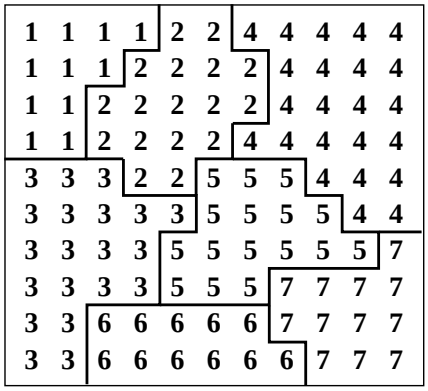

FIGURE 2. Schematic of the cellular model in two dimensions, showing cells with ID numbers 1 to 7. The difference between ID numbers corresponds to cell surface.

energy from cell-cell adhesion, elastic bulk energy from cell growth and compression from neighbors:

$$H = \sum_{sites} J_{\tau(s)tau(s')}(1 - \delta(s, s')) + \lambda_v \sum_{cells}(v_s - V_s)^2, \tag{1}$$

where J is the coupling between cells, corresponding to the adhesive energy between cell surfaces; τ represents cell type: cell adhesion strength is cell type dependent; Γ is the volume constraint coefficient, corresponding to the elastic rigidity of cells; v and V are the current cell volume and target cell volume, respectively, the latter being the volume a cell "intends" to grow to.

The cells evolve by a Monte Carlo procedure to minimize the total energy H. A cell grows in time until its volume reaches the target volume. Each cell also "carries" a cell clock. Only when the cell clock reaches the cell cycle duration and the cell volume reaches the target volume will the cell divide. The daughter cells inherit all properties of their parent with a probability for mutation.

Cells also interact with their environment, which is characterized by local concentrations of biochemicals, including nutrients (oxygen and glucose), metabolic waste (lactate), and growth promoters and inhibitors. The chemicals C_i follow the reaction-diffusion dynamics:

$$\frac{\partial C_i}{\partial t} = d_i \nabla^2 C_i - a_i. \tag{2}$$

Here the chemical (concentration C) diffuses with the diffusion constant d and is consumed (or produced) at rate a; C_0 is its concentration in the cell culture, kept constant in experiments. Each cell has its own metabolic rates, which varies as it goes through different stages of the cell cycle; thus, these metabolic rates change both in time and space. We made a few simplifying assumptions: (1) inside the spheroid the diffusion coefficients are constant, neglecting the differences of diffusion rates in extracellular matrix or cells or necrotic core; and (2) each cell is chemically homogeneous, while different cells might have different chemical concentrations; (3) the cell culture medium outside the spheroid maintains a constant level of metabolites, and (4) the external medium has no waste or inhibitory factors in it.

With these assumptions, we can solve the equations on a much coarser lattice than the lattice for cells.

The passage of a cell through its cell cycle is controlled by a series of regulatory proteins. Since experiments suggest that more than 85% of the quiescent cells are arrested in the G1 phase [**20**], in our model, the cells in their G1 phase have the highest probability of becoming quiescent. We modeled this cell-cycle arrest through a simplified protein regulatory network, based on the cell-cycle protein regulatory network for Homo sapiens [**21**], which controls the transition between G1 and S [**17**]. If the cell passes the G1-S transition checkpoint, it will most likely proceed toward mitosis. In our model, these proteins can have only 2 levels of expression — on and off. This Boolean network is designed to favor the cell transition to S phase. However, concentrations of growth and inhibitory factors directly influence the protein expression. At every time step, we calculate a local factor level:

$$\text{Factor level} = \left(1 + exp\left[-\alpha\left(\frac{gF - ihF}{initFG} - \theta\right)\right]\right)^{-1}, \tag{3}$$

where gF and ihF are current local concentrations of growth and inhibitory factors, respectively — both are outputs of the extracellular chemical equations; $initGF$ is concentration of growth factors in the medium surrounding the aggregate; θ is a factor level threshold; and α is a free parameter. If the factor level is above the threshold, the protein is turned on under two circumstances: if all the links pointing to it are stimulatory and all the proteins at the beginning of the links are on, or if all the links are prohibitory and the proteins at the beginning of the links are off. All other situations would turn off the protein. If the factor level is below the threshold, this factor level is the probability that a protein will be turned on or off — the higher the factor level (as a result of high growth factor level and low inhibitory factor level), the higher the probability of protein being turned on or off. If the outcome of this Boolean regulatory network is zero, the cell undergoes cell-cycle arrest, or turns quiescent. Otherwise, it continues its transit through the cell cycle.

Solid stress [**22**] and increased interstitial fluid pressure [**23, 24, 25, 26**] inside a solid tumor are found to inhibit cell growth in multicellular spheroids and tumors. To account for this pressure may have on the cell cycle, we included checkpoints at the end of each phase of the cell cycle to determine if the cell has increased its volume accordingly. If the cell does not increase its volume proportional to the time it has spent in that and previous phases, it will become quiescent because of pressure exerted by the surrounding tissue.

There are two sets of units in the model: lattice size and Monte Carlo steps (MCS) in the cellular model and centimeters and hours in the extracellular chemical equations. By equating a maximal cell volume in the model to a real cell size (e.g., 4x4x4 voxel = 1.2x103 μm^3), we can convert a lattice spacing to centimeters. In addition, by equating the duration of the cell cycle in the model and in real life, (e.g., 4 MCS = 12 hours), we have the conversion that 1 MCS is equal to 3 hours. With these conversions, all physical parameters can be translated to our model units, and all the model measurements can be translated into real physical units.

When a cell turns quiescent, it reduces its metabolism and stops its growth. When a cell dies, it becomes part of the necrotic core. For a short period of time (24 hours) after the cell dies by necrosis, the cell produces inhibitory factors and

some waste. In spheroid experiments, it has been observed that mitotic cells are shed from the surface of the spheroid at the constant rate per spheroid surface [**27**]. In our model, if a proliferating cell is at the surface of a spheroid of radius greater than 0.03 cm [**27**], it can shed away with a 20% shedding probability. Shed cells disappear from further consideration in the model.

We used parameters derived from spheroids using the mouse mammary tumor cells, EMT6/R0, because the experimental data for this particular cell line are abundant (e.g., [**28, 29, 30, 31, 32**]).

As the development of the solid tumor is dominated by cell growth and division, as well as the response to the microenvironment, the simulation results are not sensitive to the differences in cellular adhesion or the coupling energy coefficients J or volume constraint coefficient γ for viable cells.

3. Discussion

We report here our multiscale model that includes cellular-level descriptions of cell dynamics, intracellular level descriptions of cell-cycle regulatory network, and extracellular level descriptions of chemical dynamics. In our simulations, a single tumor cell evolves into a layered structure consisting of concentric spheres of proliferating and quiescent cells at the surface and the intermediate layer respectively, and a necrotic core at the center of the spheroid (Figure 3).

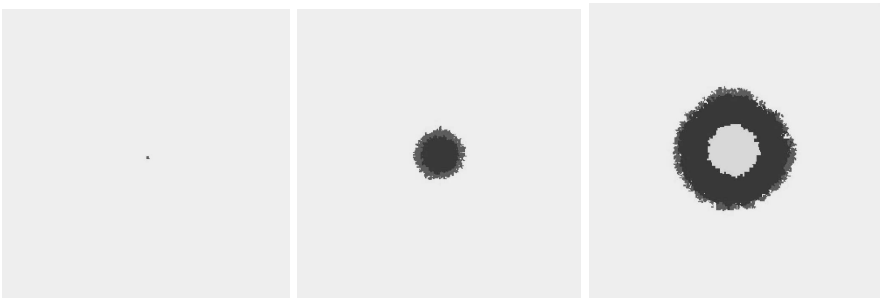

FIGURE 3. Snapshots of a simulated solid tumor at 2 days, 10 days, and 18 days of tumor growth from a single cell. Varying shades of gray correspond to proliferating, quiescent, and necrotic cells.

Figure 4 shows the comparison between the growth curves of a simulated solid tumor and two sets of spheroid experimental data. With 0.08 mM oxygen and 5.5 mM glucose kept constant in the medium, the number of cells (Figure 4a) and the tumor volume (Figure 4b) first grow exponentially in time for about 5–7 days. The growth slows down, coinciding with the appearance of quiescent cells. In both the experiments and simulations, spheroid growth saturates after around 28–30 days. We fit both the experimental and the simulation data to a Gompertz function, in order to objectively estimate the initial doubling times and the spheroid saturation sizes [**4**]. The initial volume and cell number doubling times for the experiments and the simulation differed by less than an hour (8.6–9.5 hours). The saturation sizes were more different, with the simulation overestimating the experimental maximal sizes by factors of 2 (cell number) and 2.5 (spheroid volume). Given that the

simulation covered a range of spheroid growth of 4–5 orders of magnitude, this agreement with experiment is excellent.

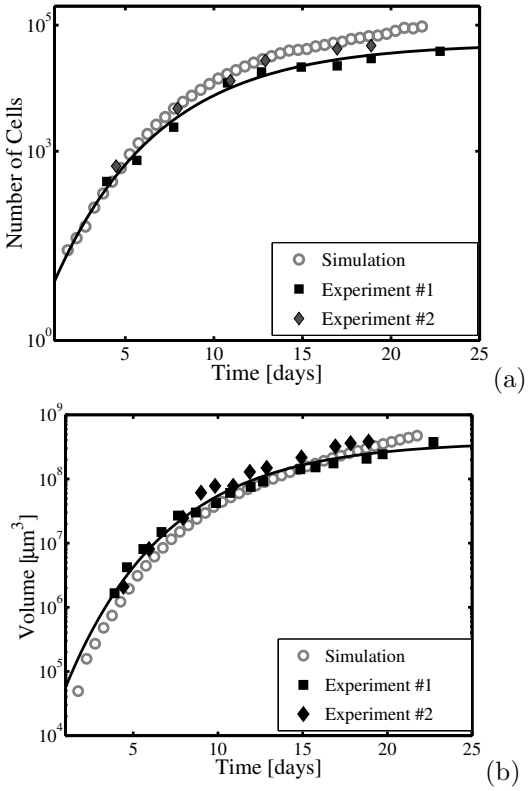

FIGURE 4. The growth curves of a spheroid with 0.08 mM O2 and 5.5 mM glucose in the medium: (a) the number of cells and (b) the volume of spheroid in time. The solid diamonds and stars are experimental data for EMT6/Ro; the circles are simulation results. The solid lines are the best fit with a Gompertz function for experimental data.

Experimentally, the fraction of cells in the various cell-cycle phases was determined by standard flow cytometric measurement of cellular DNA content as described in detail previously [**29**]. Solid symbols in Figure 5 are experimental measurements of cell cycle fraction for G1, S and G2 phases [**33**]. Open symbols are simulation data. We see in both experimental and simulation data that as the spheroid radius increases, the fraction of cells in G1 phase increases, at the same time the fraction of cells in S phase drops at comparable rate. Percent of cells in G2 phase remains roughly constant through out the spheroid growth. The simulation data showed an initially high degree of variability, mostly accounted for by the non-random distribution of the initial aggregate and the discrete time sampling involved.

In order to test the robustness of our model, we kept all the parameters in the model fixed at the values determined to produce the best fit to the growth of

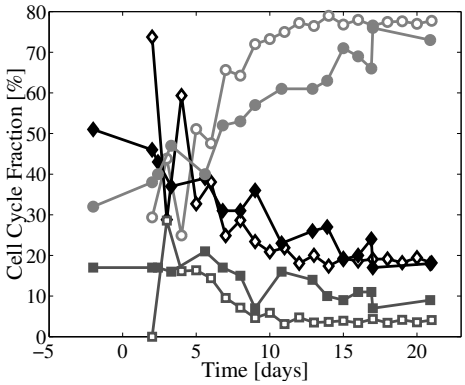

FIGURE 5. The cell cycle fraction distribution of a spheroid with 0.08 mM O2 and 5.5 mM glucose in the medium. Solid symbols are experimental data for EMT6/Ro. Open symbols are simulation results.

spheroids in 0.08 mM oxygen and 5.5 mM glucose. We then varied only the nutrient concentrations in the medium, as was done in previous spheroid experiments. Our simulations still showed good agreement between simulation and experimental growth curves when the external conditions were changed to 0.28 mM O2 and 16.5 mM glucose in the medium.

Our simulations result in a set of conditions for the cell to undergo necrosis: oxygen concentration below 0.02 mM, glucose concentration below 0.06 mM, and waste (lactate) concentration above 8 mM. While it has been shown that cells can survive these nutrient/waste concentrations individually, there are currently no experimental data available on the effects of combined exposure to these microenvironmental conditions. These simulation results suggest that cells are able to survive even in a very nutrient-deprived environment. These predictions can be tested experimentally only if chemical concentrations in the spheroid microenvironment can be systematically measured, which is difficult using currently available techniques such as microelectrodes [**32**] or bioluminescence [**34**].

The diffusion coefficients for the growth promoters and inhibitors are found to be in the order of 10^{-7} and 10^{-6} cm^2/hr, respectively. This diffusion constant range is on the order of that for peptide growth and inhibitory factors known to regulate cellular proliferation (e.g., epidermal growth factor, fibroblast growth factor, tumor necrosis factor, and tumor growth factor β) based on extrapolation from previous measurements in spheroids [**35**]. Thus, the model predicts that cellular proliferation in this system is regulated by a combination of limited growth promoters and internally produced growth inhibitors. Interestingly, previous work by Freyer et al. [**36**] has shown that a peptide inhibitory factor was produced by the necrotic regions of spheroids and that this inhibitory factor was 80–90 kD, which would have a predicted diffusion constant of $1 \times 10^{-7} cm^2/hr$ in spheroids.

It is somewhat surprising that the simplified protein regulatory network that controls cell-cycle arrest in our model could produce such a good match to the spheroid data. This result supports the idea that proliferation arrest is regulated by the induction of a few specific proteins, which act primarily in the G1-phase

of the cell cycle. The current model is entirely consistent with the recent work by our group showing that G1-specific CKIs are induced, and actively inhibit their target CDKs, relatively close to the spheroid surface [**20**]. Our modeling results also suggest that microenvironmental induction of growth arrest is not caused by restrictions on volumetric expansion of the spheroid. Even though the model incorporates such a mechanism for cell cycle arrest, the results predict that arrest is actually caused by the induction of G1-phase regulatory proteins. It is important to note that restricted volumetric growth may be an important consideration when spheroids, or nodular tumors, are surrounded by a semirigid matrix [**22**]. Our model can be further refined to include other regulatory pathways, such as the S- and G2-phase arrest, as well as to provide a finer degree of protein regulation than the on-off Boolean logic used in the current version.

4. Outlook

Despite the success of this model, we have so far only described the first phase of tumor development, the initial avascular growth. The clinically detectable tumors, typically 1–2 mm in diameter, are near growth saturation, when many of the cellular and microenvironmental perturbations that drive tumor progression, including alterations in metabolism, gene, and protein expression and proliferation arrest, have maximal effects. Furthermore, angiogenesis is necessary for a tumor to grow beyond saturation. A predictive model of tumor growth must cover longer times and length scales.

We are currently expanding the model to simulate the initiation of angiogenesis. Additional ingredients to the avascular tumor growth model described above include vascular endothelial cells, their interaction with the local angiogenic signal — in particular the vascular endothelial growth factor (VEGF) generated by the tumor — and their interaction with the extracellular matrix among the tissue between the blood vessel and the tumor.

The vascular endothelial cells would not only increase proliferation, decrease apoptosis rate, but also migrate towards the higher concentration of the VEGF signal (or chemotaxis) [**37**]. In our model, we do not consider endothelial cell death. The endothelial chemotaxis is modeled with an effective chemical potential term in the total energy:

$$H = \sum_{sites} J_{\tau(s)tau(s')}(1 - \delta(s, s')) + \lambda_v \sum_{cells} (v_s - V_s)^2 + \sum_{cells} \mu C_c, \tag{4}$$

where μ is the chemical potential corresponding to the cell's capability to follow a chemical gradient or chemotaxis, and C_c is the local concentration of the chemoattractant. When the cellular model minimizes the total energy, the cells would move toward higher values of C if μ is negative. The dynamics of VEGF is similar to those of the chemicals in the above avascular model, the only difference being that VEGF also decays in time and the source of VEGF is localized at the tumor.

Collagens are the major proteins of the ECM [**38**]. The family of collagen molecules are typically long (300 nm), thin (1.5 nm) fibers [**39**]. We model the extracellular matrix as a matrix of fibers (see Fig. 4(a)). They are a special "cell" with a target volume and rigidity, as well as a adhesion coupling with the cells. The interstitial fluid between the fibers are treated as another special "cell" with its target volume and rigidity. The space occupied by interstitial fluid is more deformable than the fibers and is more easily "invaded" by the expanding and

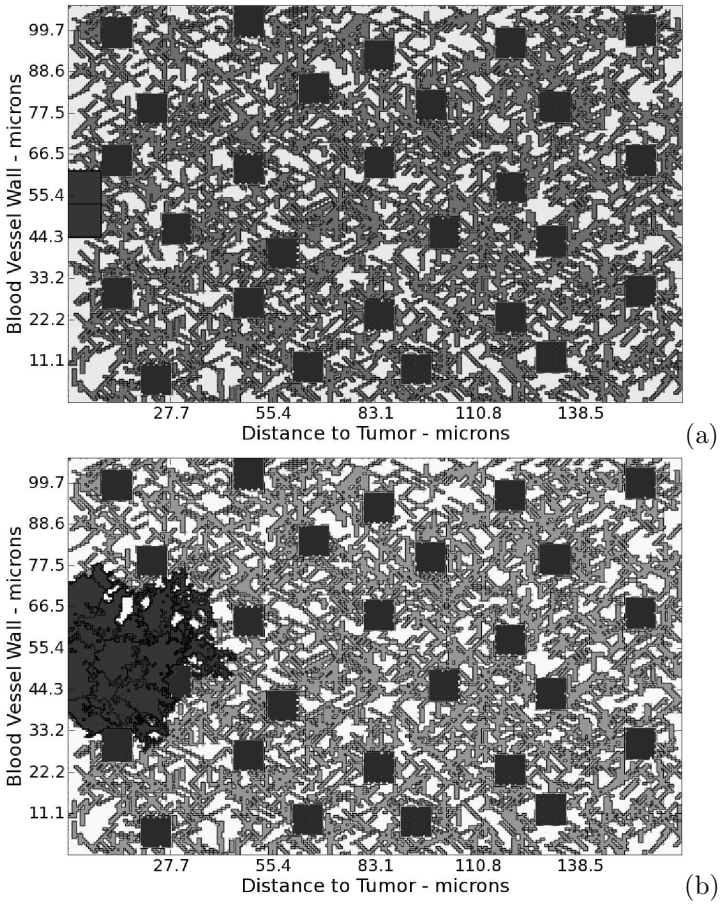

FIGURE 6. Simulation of two dimensional angiogenesis. The left edge of the simulation domain is the blood vessel wall, while the right edge is the source of VEGF. The endothelial sprout initially consists of two endothelial cells (dark gray). Endothelial cells grow and migrate in the normal tissue consists of normal cells (gray squares), matrix fibers and interstitial fluids (light gray). (a) Initial condition at time 0. (b) At about 5 days.

migrating endothelial cells. Normal tissue cells occupy around 12.5% of space. When growing endothelial sprout compresses the normal cells, they can undergo apoptosis and become part of the interstitial fluid.

The interactions between the endothelial cells and the extracellular matrix contain two aspects. One involves the active role of the endothelial cells in modifying the local fibronectin concentration and re-organizing the fiber structure; the other is the passive role of the endothelial cells by haptotaxis or the cells' response in a gradient of adhesion from the gradient of fibronectin density. We treat the former by a set of local rules for endothelial cells: if the matrix element around the cell is lower than a threshold—matrix density too low, the cell secretes a fixed amount

of matrix; if the matrix element around the cell is higher than another threshold—matrix density too high, the cell secretes an enzyme that degrades the local matrix fibers. Haptotaxis in this model comes through the different coupling constants J in the first term of total energy.

It has been established that endothelial cells either migrate or divide, but not both [**9**]. We treat the endothelial sprout tip as a group of cells that only migrate but do not proliferate. Cell division is largely confined to a region just behind the cluster of cells that constitute the sprout tip. This division region, however, has not been generally agreed on. Evidence also pointed to " some cell-wide distances behind, particularly at the base of the sprout. [**40, 41**]. We shall explore different possibilities and their effects on angiogenesis.

Additional considerations that could be added to the model are intracellular regulations for endothelial cells, and the active role of matrix in storing and releasing VEGF. Our preliminary results (Figure 4) have shown that this method for simulating angiogenesis is promising.

In addition, we also embed blood vessels into the tumor to study the vascular tumor growth as well as the effects of chemotherapy on vascular tumor growth. This multiscale approach, combined with the extant data, will help construct anatomically accurate models of a tumor and its vascular system. If successfully implemented, the model can guide experimental design and interpretation. Continuously revised by new information, the final model could potentially enable us to assess tumor susceptibility to multiple therapeutic interventions, improve understanding of tumor biology, better predict and prevent tumor metastasis, and ultimately increase patient survival.

Acknowledgment

References

[1] Jemal, A. The Journal of the American Medical Association, 294: 1255-1259 (2005).
[2] Sutherland, R.M. Cell and environment interactions in tumor microregions: the multicell spheroid model. Science 240: 177-184 (1988).
[3] Knighton, D., D. Ausprunk, D. Tapper, and J. Folkman. Avascular and vascular phases of tumor growth in the chick embryo. British J. Can. 35. 347-356 (1977).
[4] Marusic, M., Z. Bajzer, J.P. Freyer and S. Vuk-Pavlovic. Analysis of growth of multicellular tumour spheroid by mathematical models. Cell Prolif. 27. 73 (1994).
[5] Greenspan, H.P. On the growth and stability of cell cultures and solid tumors. J. Theor. Biol. 56, 229. (1976).
[6] Friedman, A. and F. Reitich. Analysis of a mathematical model for the growth of tumors. J. Math. Bio. 38, 262-284 (1999).
[7] Sherrat, J.A., and M.A.J. Chaplain. A new mathematical model for avascular tumor growth. J. Math. Biol. 43: 291-312 (2001).
[8] Moreira, J. and A. Deutsch. Cellular automaton models for tumor development: A critical review. Advances in Complex Systems. 5, 247 (2002).
[9] Anderson, ARA. and MAJ Chaplain. Continuous and discrete mathematical models of tumor induced angiogenesis. Bull. Math. Biol. 60, 587 (1998).
[10] Jackson, T.L., and H.M Byrne, Mathematical Model to Study the Effects of Drug Resistance and Vasculature on the Response of Solid Tumors to Chemotherapy Math. Biosci. 164, 17-38 (2000).
[11] Jackson, T.L. Intracellular Accumulation and Mechanism of Action of Doxorubicin in a Spatio-Temporal Tumor Model J. Theor. Biol. 220(2) 201-213 (2003).
[12] Kevrekidis, P.G. Whitaker, N. and Good D.J. Towards a reduced model for angiogenesis: A hybrid approach. Math & Com. Model. 41: 987-996. (2005).

[13] McDougall, S.R., A.R. Anderson. MAJ Chaplain, and J.A. Sherratt. Mathematical model of flow through vascular networks: implications for tumor-induced angiogenesis and chemotherapy strategies. Bull. Math. Biol. 64. 673-702 (2002).
[14] Zheng, X., S.M. Wise, and V. Cristini. Nonlinear simulation of tumor necrosis, neovascularization and tissue invasion via an adaptive finite-element/level-set method, Bull Math Biol 67(2): 211-259 (2005).
[15] Alarcon, T., H.M. Byrne, and P.K. Maini. A Multiple Scale Model for Tumor Growth, Multiscale Modeling and Simulation. 3: 440-475 (2004).
[16] Alarcon, T., H.M. Byrne, and P.K. Maini. Towards whole-organ modelling of tumour growth, Progress in Biophysics & Molecular Biology. 85: 451 - 472 (2004).
[17] Jiang, Y., J. Pjesivac, C. Cantrell, and J. Freyer. A multiscale model for avascular tumor growth, Biophys. J. 89 (2005).
[18] Glazier, J.A. and F. Garner. Simulation of the differential adhesion driven rearrangement of biological cells. Phys. Rev. E 47: 2128-2154 (1993).
[19] Jiang, Y., H. Levine and J. A. Glazier, Differential adhesion and chemotaxis in mound formation of Dictyostelium, Biophys. J. 75, 2615 (1998).
[20] LaRue, K.E., M. Kahlil, and J.P. Freyer. Microenvironmental regulation of proliferation in EMT6 multicellular spheroids is mediated through differential expression of cycline-dependent kinase inhibitors. Cancer Res. 64, 1621 (2004).
[21] Data from the Kyoto Encyclopedia of Genes and Genomes (kegg.com).
[22] Helmlinger, G., P.A. Netti, H.C. Lichtenbeld, R.J. Melder, and R.K. Jain. Solid stress inhibits the growth of multicellular tumor spheroids. Nature Biotechnology. 15: 778-783 (1997).
[23] Sarntinoranont, M, F. Rooney, and M. Ferrari. Interstitial stress and fluid pressure within a growing tumor. Annal. Biomed. Engineer. 31: 327-335 (2003).
[24] Boucher, Y., L.T. Baxter, and R.K. Jain. Interstitial pressure gradients in tissue-isolated and subcutaneous tumors: implications for therapy. Cancer Res. 50: 4478-4484 (1990).
[25] Boucher, Y., J. Salehi, B. Witwer, G.R. Harsh, and R.K. Jain. Interstitial fluid pressure in intracranial tumors in patients and in rodents. Br. J. Cancer 75: 829-836 (1990).
[26] Gutmann, R., M. Leunig, J. Feyh, A.E. Goetz, K. Messmer, E. Kastenbauer, and R.K. Jain. Interstitial hypertension in head and neck tumors in patients: correlation with tumor size. Cancer Res. 52: 1993-1995 (1992).
[27] Landry, J., J.P. Freyer, and R.M. Sutherland. A model for the growth of multicellular tumor spheroids. Cell Tiss. Kinet. 15: 585-594 (1982).
[28] Freyer, J.P. and R.M. Sutherland. Regulation of growth saturation and development of necrosis in EMT6/R0 multicellular spheroids by the glucose and oxygen supply. Cancer Res. 46: 3504-3512 (1986).
[29] Freyer, J.P. and R.M. Sutherland. Proliferative and clonogenic heterogeneity of cells from EMT6/Ro multicellular spheroids induced by the glucose and oxygen supply. Cancer Res. 46: 3513-3520 (1986).
[30] Freyer, J.P. and R.M. Sutherland. A reduction in the in situ rates of oxygen and glucose consumption of cells in EMT6/R0 spheroids during growth. J. Cell. Physiol. 124: 516-524 (1985).
[31] Freyer, J.P. Rates of oxygen consumption for proliferating and quiescent cells isolated from multicellular tumor spheroids. Adv. Exp. Med. Biol. 345: 335-342 (1994).
[32] Mueller-Klieser, W., J.P. Freyer, and R.M. Sutherland. Influence of glucose and oxygen supply conditions on the oxygenation of multicellular spheroids. Br. J. Cancer 53: 345-353 (1986).
[33] Freyer, J.P. Role of necrosis in regulating the growth saturation of multicellular spheroids. Cancer Res. 48: 2432-2439 (1988).
[34] Walenta, S., J. Doetsch, W. Mueller-Klieser, and L. Kunz-Schughart. Metabolic imaging in multicellular spheroids of oncogene-transfected fibroblasts. J. Histochemistry & Cytochemistry. 48: 509-522 (2000).
[35] Freyer, J.P. and R.M. Sutherland. Determination of diffusion constants for metabolites in multicell tumor spheroids. Adv. Exp. Med. Biol. 159: 463-475 (1983).
[36] Freyer, J.P., P.L. Schor, and A.G. Saponara. Partial purification of a protein growth inhibitor from multicellular spheroids. Biochem. Biophys. Res. Comm. 152: 463-368 (1988).
[37] Lobov, I.B. , P.C. Brooks, and R.A. Lang, Angioproietin-2 displays VEGF-dependent modulation of capillary structure and endothelial cell survival in vivo. Proc. Natl. Acad. Sci. USA, 99, 17:11205-11210 (2002).

[38] Alberts, B., D. Bray, J. Lewis, M. Raff, K. Roberts, J.D. Watson. *Molecular Biology of the Cell*, Third Edition, Garland Science, NY, 1994.
[39] Loewy, A.G., P. Siekevitz, J. R. Menninger, J.A.N. Gallant. *Cell Structure and Function: An Integrated Approach*, Third Edition, Saunders College Publishing, Philadelphia PA, 1991.
[40] Paweletz, N, M. Knierim. Tumor-related angiogenesis. Crit. Rev. Oncol. Hematol. 9: 197–242 (1989).
[41] Orme ME, MA Chaplain. A mathematical model of the first steps of tumor-related angiogenesis: capillary sprout formation and secondary branching. IMA J. Math Appl. Med Biol. 13:73–98 (1996).

Theoretical Division, Los Alamos National Laboratory, Los Alamos, NM 87545